# Effect of the Liquid Injection Angle on the Atomization of Liquid Jets in Subsonic Crossflows

H. Almeida, J. M. M. Sousa and M. Costa*
Mechanical Engineering Department, Instituto Superior Técnico
Technical University of Lisbon
Avenida Rovisco Pais, 1049-001 Lisboa, Portugal

**Abstract**

This work focused on the study of sprays produced by pressure atomizers of single-hole type when subjected to air crossflows at atmospheric pressure. The study was carried out in a wind tunnel. Prior to spray characterization, the air flow inside the wind tunnel was evaluated with the use of laser Doppler anemometry. The sprays were first characterized using shadowgraph, which allowed a qualitative evaluation of the overall quality of atomization. Subsequently, the use of phase Doppler anemometry allowed performing detailed measurements of the spray droplet diameters and the two velocity components as a function of the injection angle. The main findings of this study are as follows: i) the liquid column disintegration process is significantly affected by the liquid injection angle and, less considerably, by the liquid to air momentum flux ratio ii) the SMD values decrease noticeably as the injection angle of the liquid increases; iii) the characteristics of droplet diameter and velocity distributions vary significantly with the distance to the injector.

## Introduction

The atomization of liquids in air crossflows is an important topic in the areas of combustion, agriculture and pharmaceutical industry. For example, in the case of combustion, some combustors for gas turbines use the fuel injection (gas or liquid) in a recirculation region of combustion products [e.g., 1, 2]. In practical terms, this requires the fuel to be injected by pressure atomizers (in the case of liquid fuels) from the combustion chamber walls, thus forming an angle with the main flow inside. It is therefore important to study the sprays characteristics produced by this type of atomizers in air crossflows. There are, however, very few studies available in literature concerning this area of atomization, and the vast majority only considers cases where the liquid is injected at an angle of 90º with respect to the crossflow. Furthermore, the use of liquid angled injection (i.e., where the liquid is injected at angles smaller than 90º with respect to the gas phase crossflow) is very common in combustion, agriculture and pharmaceutical application areas. Hence, this paper aims at extending the present knowledge in this area of liquid jets atomization.

Relevant related studies of round liquid jets in gaseous subsonic crossflows included those of references [3-11]. These works have determined liquid column trajectories, column fracture locations, and near-field spray characteristics as a function of the liquid injection angle, $\alpha$. An important conclusion of these studies was that the liquid column trajectories correlate well with $\alpha$ and liquid-to-air momentum flux ratio, $q$.

With the exception of Fuller *et al.* [6], Costa *et al.* [10] and Bellofiore *et al.* [11], the available studies in the literature only consider the case where the liquid is injected with at an angle of 90º with respect to air crossflow. Additionally, only Costa *et al.* [10] have made use of phase Doppler anemometry to carry out a detailed characterization of the sprays as a function of the injection angle, although this study has been conducted for relatively low crossflow velocities. In this context, it is important to enhance the knowledge regarding angled injection of liquid sprays in crossflows at higher velocities.

The main objective of this work consists on the characterization of sprays produced by single-hole pressure atomizers, when subjected to subsonic air crossflows at atmospheric pressure conditions. The study was conducted in a wind tunnel, where the air flow was previously characterized with the use of laser Doppler anemometry (LDA). Subsequently, the spray characterization was carried out using shadowgraph and phase Doppler anemometry (PDA).

## Materials and Methods

Fig. 1 shows schematically the test section, including details of the atomizer geometry, and of the diagnostics. The wind tunnel used was built in glass with the following dimensions: length $L$ = 0.500 m, height $H$ = 0.075 m and width $W$ = 0.050 m. A honeycomb was installed in the plenum, upstream a 24:1 contraction, in order to eliminate large-scale vortices. The contraction was designed according to the methodology proposed by

*Corresponding author: mcosta@ist.utl.pt

Tulapurkara and Bhalla [12] aiming to minimize both non-uniformities in the mean flow and turbulence intensity in the test section.

In this study, four single-hole pressure atomizers were used, corresponding to injection angles $\alpha$ of 30º, 45º, 60º and 90º. The atomizer internal diameter, $d$, was constant and equal to 0.15 mm. The ratio between the length of the discharge hole and the inner diameter of the atomizer was, in all cases, larger than 100, which ensures that the liquid flow is fully developed at the discharge. For security reasons, the liquid used in the tests was distilled water, which was fed from a pressurized tank at 15 bar using nitrogen bottles. The setup allowed characterizing the sprays produced by the four atomizers as a function of the injection angle ($\alpha$), the liquid injection velocity ($V_{liq}$) and the air crossflow velocity ($U_g$). Fig. 2 shows the coordinate system used in the present study.

A commercial LDA system (DANTEC, Denmark) was used to characterize the air flow in the wind tunnel, measuring the two velocity components simultaneously in dual-beam backward scattering operation mode. To generate the seeding particles, four medical nebulizers Inspiron 002305 were used, employing a mixture of water (20%) and ethylene glycol (80%). The analogue signal from the photomultipliers was band-pass filtered and processed by two burst spectrum analyzers model DANTEC 57N20/57N35, using an IEEE interface with a computer. With this configuration it was possible to collect data samples at an average acquisition rate of about 0.5 kHz. Mean velocities and their variances were computed by ensemble averaging from 10000 samples, using DANTEC BSA Flow Software.

Initially, the characterization of the sprays involved the use of an interferometric technique called shadowgraph. To that end, an argon-ion laser emitting at a wavelength of 515 nm with a maximum power of 500 mW was employed. The spray zone images were recorded by a high-speed digital camera, model Phantom v4.2 (Vision Research, USA), with a resolution of 512×512 pixels (monochrome sensor with sensitivity 4800 ISO/ASA), using exposure times of 10 ms and average acquisition periods of about 66 ms. The lens used was a model AF Micro-Nikkor 60 mm f/2.8D (NIKON, Japan). As a result of the optical arrangements used during the experiments, the spatial resolution was limited to ≈ 125 μm/pixel. For the management of final digital images, built-in MATLAB® routines were employed.

After the visualization, droplet diameters and velocities in the sprays were quantified by the use of PDA. Similarly to the LDA, a commercial two-component DANTEC system was employed (see Fig. 1). In this case, the receiving probe was positioned at an angle with the transmitting optics not very far from Brewster's refraction angle, which corresponded to 73.7º. This allowed taking advantage of the dominance of the first-order of refraction of light in the droplets and, at the same time, reducing the influence of higher-order refractions. The optical arrangement produced a measuring volume approximately 4 mm in length and 2 mm in diameter. The optical receiver was adjusted for "medium-sized particles" (mask B) and positioned at an angle of 59º, allowing to measure droplet diameters up to nearly 400 μm. The analogue signals from the photomultipliers produced by the scattered light were processed by a module interface model DANTEC P80.

The determination of the statistical distribution of diameters and velocities of drops was made using again DANTEC BSA Flow Software. In the process of validating the signal, the signal-to-noise ratio and deviations from sphericity were taken into account. The sphericity criterion was always set to 15%. The number of samples in the measurements was generally larger than 5000, though in areas characterized by high acquisition rates this number has reached 10,000. Based on the analysis of these sources of error it is estimated that the overall uncertainty in the measurement of mean velocities is below 2%. In the case of droplet diameters, the overall uncertainty is estimated to be approximately 5%.

**Results and Discussion**

Table 1 summarizes the operating conditions employed in the present study.

Fig. 3 shows the mean velocity and turbulent kinetic energy profiles in the wind tunnel, measured at the section where the discharge hole of the atomizer was located. The profiles were normalized using the potential flow velocity, $U_{air}$, as a velocity scale, and using the height, $H$, and the width, $W$, of the tunnel as length scales. Since measurements of the third velocity component were not performed, the turbulent kinetic energy was calculated via estimation of the third velocity variance as the semi-sum of its counterparts, which is a good approximation in boundary layer flows [13].

Fig. 3a shows a typical behaviour of a boundary layer flow, displaying high velocity gradients in the near-wall region. It was found that the boundary layer thickness varied slightly with the operating conditions of the wind tunnel, remaining always close to 4 mm. The same can be said about the displacement thickness (approximately between 0.36 and 0.40 mm) and the momentum thickness (approximately between 0.29 and 0.33 mm), resulting in a nearly constant value of the shape factor, close to 1.2.

The homogeneity of the velocity profiles outside the boundary layer can also be observed, showing that the purpose for which the contraction was projected was achieved. Also, the turbulent kinetic energy exhibits a maximum near the wall, which is associated to the high gradients of the mean velocity, but declined significantly to approximately constant values outside the boundary layer. The turbulence intensity exhibited a nearly negligible

dependence of the operating conditions, settling at ≈ 2%. The three-dimensional character of the air flow the wind tunnel can be judged from the measured transverse profiles shown in Fig. 3b for different distances to the wall (wind tunnel floor). Although the flow in a tunnel of rectangular section will inevitably show some three-dimensional characteristics, these effects are mainly noted at the corners presumably due to the establishment of Prandtl's secondary flow of the second kind. It appears that the observed gradients of mean velocity and turbulent kinetic energy that occur in the central plane of the tunnel (where the liquid is injected) are very small and, therefore, its influence in the process of atomization is expected to be minimal.

Fig. 4 shows instantaneous spray images that reveal the effect of the liquid injection angle on the atomization process. It can be seen that the spray opening angle increases with the liquid injection angle, $\alpha$: the larger the injection angle, the greater the droplets dispersion. This is a consequence of the fact that as the injection angle decreases, the relative velocity, $\bar{u}_{rel}$, also decreases. Specifically, when $\alpha$ decreases from 90º to 30º, $u_{\mathrm{rel}}$ decreases from 1 to 0.94 (Table 1). Consequently, by decreasing $\alpha$, while maintaining $q$ constant, a reduction of the aerodynamic forces acting on the exposed area of the liquid column is achieved. As shown in Fig. 4, as $\alpha$ decreases, the disintegration process becomes less effective. These spray images show a behaviour somewhat similar to that described by Fuller *et al.* [6], regarding the variation in the quality of the sprays as a function of the liquid injection angle.

Figs. 5 to 8 show normalized velocities and droplet size along the $y$-direction for test conditions 1, 2, 3 and 4 at $x/d$ = 50, 100, 200, 400 and 800, respectively. A comparison between the evolutions presented in these figures allows assessing the influence of the liquid injection angle in velocities and droplet size. It appears that as $\alpha$ increases, the values of SMD decrease significantly. Again, this behaviour may be attributed to the higher $u_{\mathrm{rel}}$ values associated to the larger liquid injection angles, hence to the growing aerodynamic forces acting on the liquid surface.

Fig. 9 shows normalized velocities and droplet size along the spray centerline (location detected by the maximum mass flux indicated by the PDA) for test conditions 1, 2, 3 and 4. It is observed that the atomization process ends approximately at $x/d$ = 1000 for test condition 1, at $x/d$ = 800 for test condition 2, at $x/d$ = 550 for test condition 3 and at $x/d$ = 450 for test condition 4. Fig. 10 shows droplet size distributions along the spray centerline for test condition 2 at $x/d$ = 400, 500, 600, 700 and 800.

Fig. 11 shows droplet velocity and size distributions in various spray locations for test condition 2. The figure revels that there is a significant difference between the droplet distributions obtained in the top regions of the spray for $x/d$ = 50 and those obtained in other locations, both vertical and longitudinal. Corresponding distributions exhibit two distinct populations: the first (dominant), characterized by mean velocities lower than 40 m/s, that is associated to the ligaments and large drops occurring in these regions of particularly dense spray; and the second, characterized by mean velocities close to 60 m/s, associated to small droplets formed at the initial stage of disintegration of the liquid jet (surface breakup), that are more easily accelerated by the air crossflow. Such characteristic is almost imperceptible at $x/d$ = 100 and further downstream, where the velocity distributions exhibit an essentially symmetrical character and the corresponding mean velocities approach the air flow velocity. Concerning droplet diameters, a significant change in the character of these distributions can be observed occurring at $x/d$ = 100. At this station, more uniform droplet size distributions begin to emerge (at the bottom of the spray), showing a significant reduction on the amount of large droplets, which dominated the spray at upstream locations. However, it must be noted that although the counting of the latter droplets may not be very high, their contribution by mass or volume is probably dominant, as a result of the cubic dependence with the droplet diameter, which translates into the large values of SMD already presented in Figs. 5 to 8. As expected, the above-described characteristic becomes stronger with increasing distance from the injector, as a result of the natural evolution of the atomization process.

**Conclusions**

The main findings of this study are as follows:

1. The disintegration process of the liquid columns is significantly affected by the liquid injection angle and, to a lesser extent, by the liquid-to-air momentum flux ratio. As the liquid injection angle was decreased, the atomization process degraded as a result of a reduction in the aerodynamic forces acting on the exposed surface of the liquid column. A similar effect was obtained by increasing the liquid-to-air moment flux ratio.
2. The values of the SMD decreased significantly with the increase of the liquid injection angle as a consequence of the resulting higher values of the relative velocity of the air and, therefore, due to fact that the aerodynamic forces acting on the liquid surface of the jet increase with the injection angle.
3. There is a significant difference between the droplet velocity distributions observed in the top regions of the spray for $x/d$ = 50 and those obtained in other locations, both vertical and longitudinal. In the former, the corresponding distributions exhibit two distinct populations: the first, characterized by mean velocities lower than 40 m/s, that is associated to the ligaments and large drops occurring in these regions of particularly dense spray; and the second, characterized by mean velocities close to 60 m/s, associated to small

drops formed at the initial stage of disintegration of the liquid jet, that are more easily accelerated by the air crossflow.

4. A significant change in the character of the droplet diameter distributions was observed at $x/d$ = 100. At this station, more uniform droplet size distributions begin to emerge, showing a significant reduction on the amount of large droplets, which dominated the spray at upstream locations. This characteristic becomes stronger with increasing distance from the injector, as a result of the natural evolution of the atomization process.

**Nomenclature**

| | |
|---|---|
| $d$ | nozzle diameter |
| $H$ | wind tunnel height |
| $k$ | air turbulent kinetic energy |
| $L$ | breakup length |
| $Oh$ | Ohnesorge number, $\mu_{liq}/(\rho_{liq} d\, \sigma_{liq})^{1/2}$ |
| $q$ | liquid-to-air momentum flux ratio, $\rho_{liq} V_{liq}^2/(\rho_{air} U_{air}^2)$ |
| $Re_{air}$ | freestream Reynolds number, $\rho_{air} U_{air} d/\mu_{air}$ |
| $Re_{liq}$ | liquid jet Reynolds number, $\rho_{liq} V_{liq} d/\mu_{liq}$ |
| $SMD$ | Sauter mean diameter |
| $u$ | velocity in $x$-direction |
| $u_{rel}$ | relative air velocity, $(U_{air}-u_{liq})/U_{air}$ |
| $U_{\mathrm{air}}$ | air velocity of the crossflow |
| $v$ | velocity in $y$-direction |
| $V_{liq}$ | liquid injection velocity |
| $W$ | wind tunnel width$We_{rel\text{-}air}$relative air Weber number, $\rho_{air} d(U_{air}-u_{liq})^2/\sigma$ |
| $We_{liq}$ | liquid Weber number, $\rho_{liq} d\, V_{liq}^2/\sigma_{liq}$ |
| $x, y, z$ | coordinates |
| $\alpha$ | liquid injection angle |
| $\mu$ | dynamic viscosity |
| $\rho$ | density |
| $\sigma$ | liquid surface tension |

Subscripts

| | |
|---|---|
| $air$ | air property |
| $liq$ | jet exit liquid property |
| $p$ | particle/droplet |

**References**


[1] Roquemore, W. M., Shouse, D., Burrus, D, Johnson, A., Cooper, C., Duncan, B., Hsu, K. Y., Katta, V. R., Sturgess, G. J., Vihinen, I., *AIAA Paper* 2001-0483 (2001).

[2] Melo, M. J., Sousa, J. M. M., Costa, M., Levy, Y., *Journal of Propulsion and Power* 25:609-617 (2009).

[3] Inamura, T., and Nagai, N., *Journal of Propulsion and Power* 13:250-256 (1997).

[4] Wu, P. K., Kirkendall, K. A., Fuller, R. P., Nejad, A. S., *Journal of Propulsion and Power* 13:64-73 (1997).

[5] Wu, P. K., Kirkendall, K. A., Fuller, R. P., Nejad, A. S., *Journal of Propulsion and Power* 14:173-181 (1998).

[6] Fuller, R. P., Wu, P.K., Kirkendall, K. A., Nejad, A. S., *AIAA Journal* 38:64-72 (2000)..

[7] Becker, J., and Hassa, C., *Atomization and Sprays* 11:49-67 (2002).

[8] Cavaliere, A., Ragucci, R., Noviello, C., *Experimental Thermal and Fluid Science* 27:449-454 (2003).

[9] Sallam, K. A., Aalburg, C., Faeth, G. M., *AIAA Journal* 42:2529-2540 (2004).

[10] Costa, M., Melo, M. J., Sousa, J. M. M., Levy, Y., *AIAA Journal* 44:646-653 (2006).

[11] Bellofiore, A., Cavaliere, A., Ragucci, R., *Combustion Science and Technology* 179:319-342 (2007).

[12] Tulapurkara, E. G., and Bhalla, V. V. K., *ASME Journal Fluids Engineering* 110:45-47 (1988).

[13] Spalart, P. R., *Journal of Fluid Mechanics* 187:61-98 (1988).

**Table 1.** Operating conditions[a].

| Test condition | $\alpha$ (deg.) | $We_{rel\text{-}air}$ | $u_{rel}$ | $q$ |
|---|---|---|---|---|
| 1 | 30 | 29 | 0.94 | 4.37 |
| 2 | 45 | 30 | 0.95 | 4.37 |
| 3 | 60 | 31 | 0.96 | 4.37 |
| 4 | 90 | 33 | 1.00 | 4.37 |

[a] For all test conditions: $d$ = 0.15 mm, Oh = 0.0084, $V_{liq}$ = 8.2 m/s, $Re_{liq}$ = 1424, $We_{liq}$ = 144, $U_{air}$ = 116.7 m/s, $Re_{air}$ = 1064.

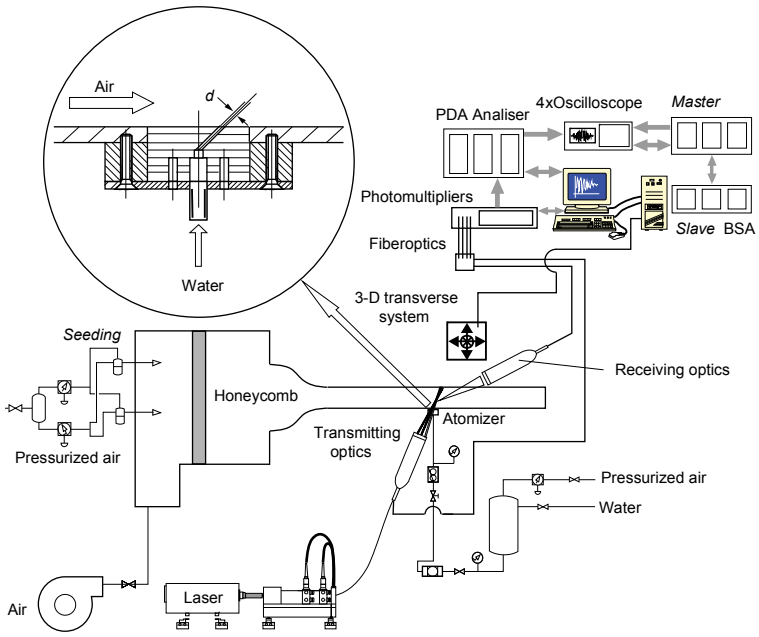


**Figure 1.** Schematics of the test section, including details of the atomizer geometry, and of the diagnostics.

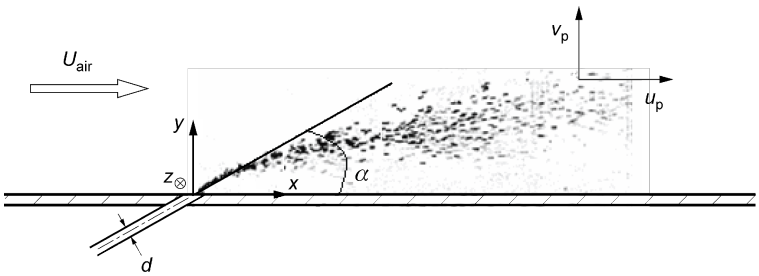


**Figure 2.** Coordinate system.

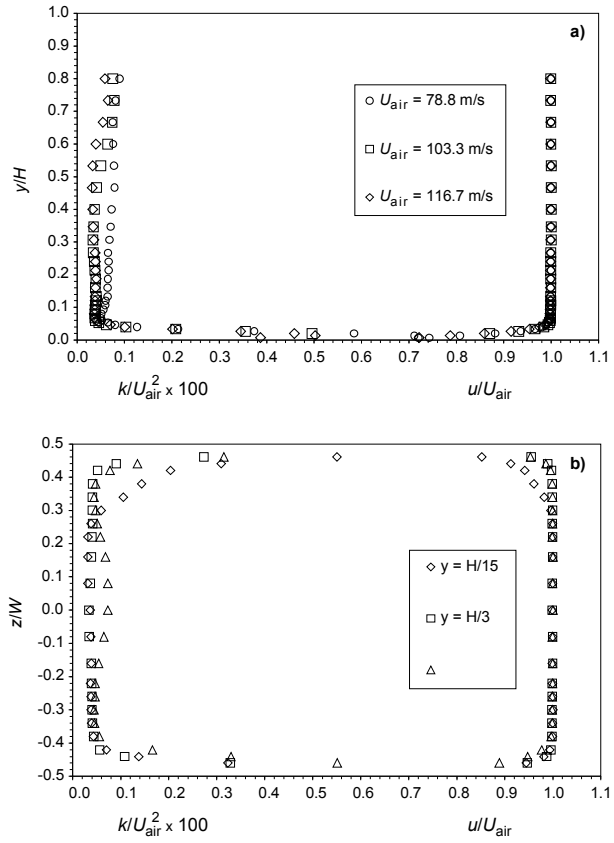


**Figure 3.** Mean velocity and turbulent kinetic energy profiles in the wind tunnel: a) vertical profiles; b) transverse profiles.

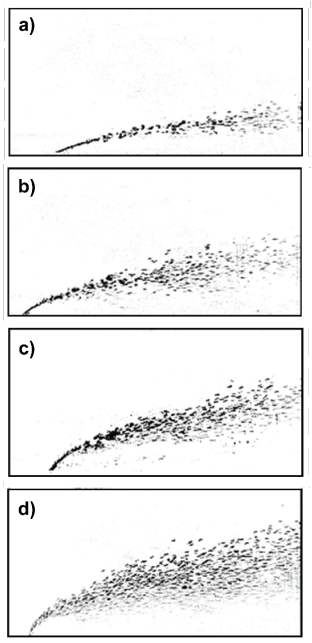


**Figure 4.** Instantaneous spray images showing the effect of the liquid injection angle on the atomization process: a) test condition 1; b) test condition 2; c) test condition 3; d) test condition 4.

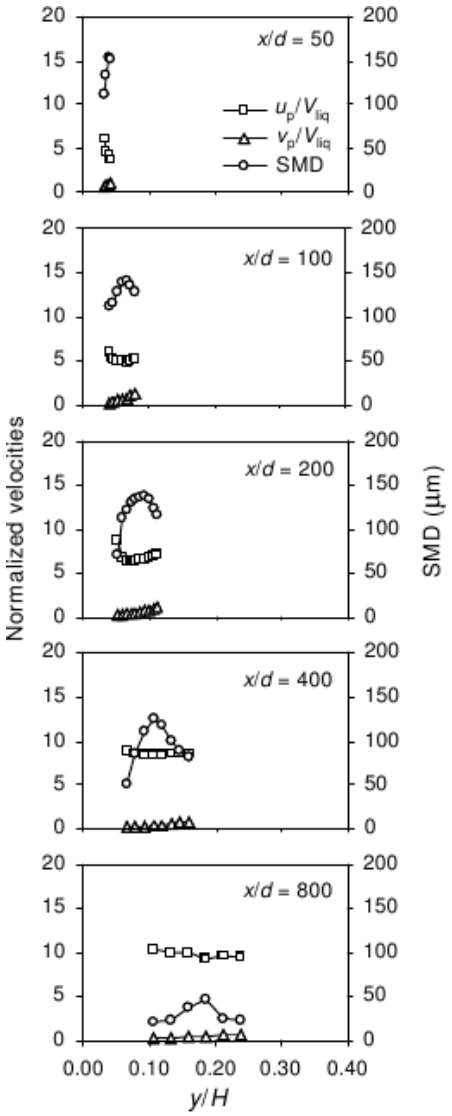


**Figure 5.** Normalized velocities and droplet size along the *y*-direction for test condition 1 ($\alpha$ = 30º) at $x/d$ = 50, 100, 200, 400 and 800.

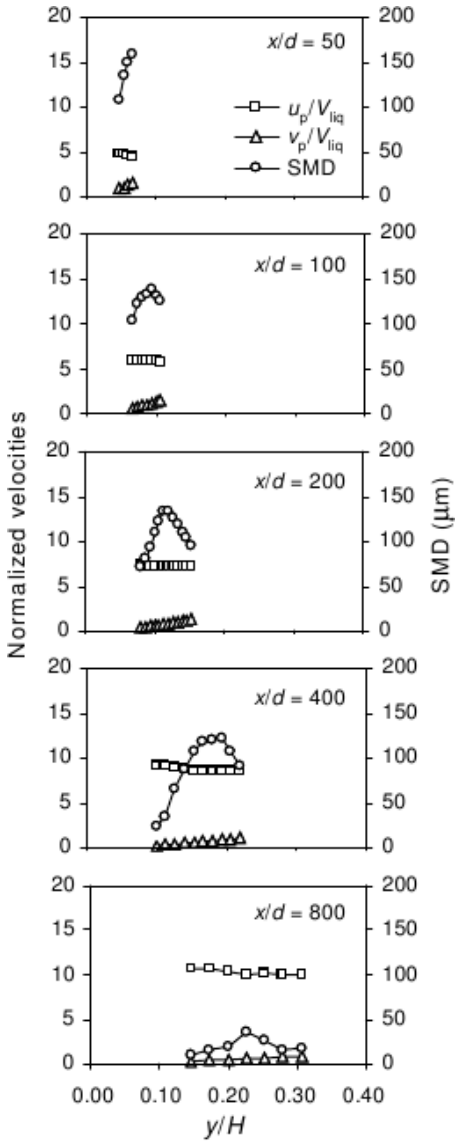


**Figure 6.** Normalized velocities and droplet size along the *y*-direction for test condition 2 ($\alpha$ = 45º) at $x/d$ = 50, 100, 200, 400 and 800.

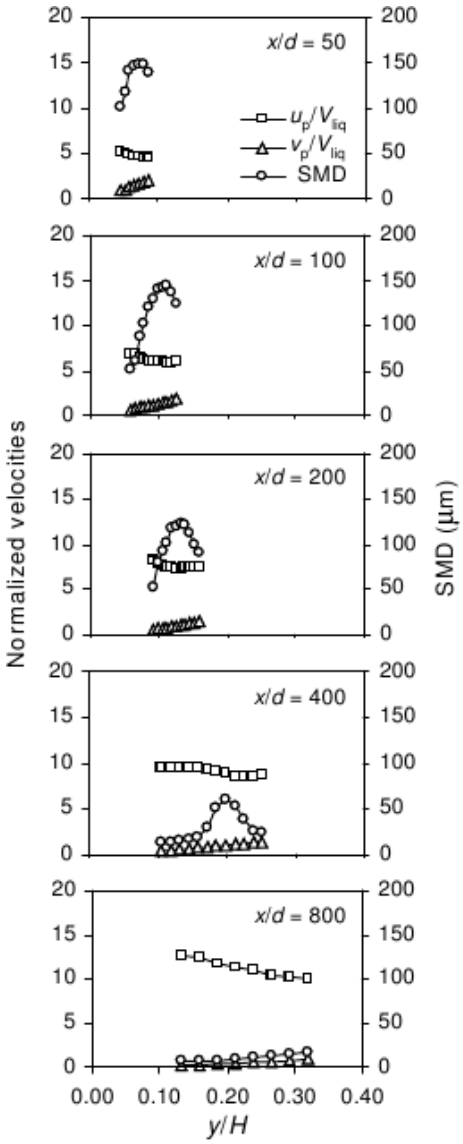


**Figure 7.** Normalized velocities and droplet size along the *y*-direction for test condition 3 ($\alpha = 60º$) at $x/d$ = 50, 100, 200, 400 and 800.

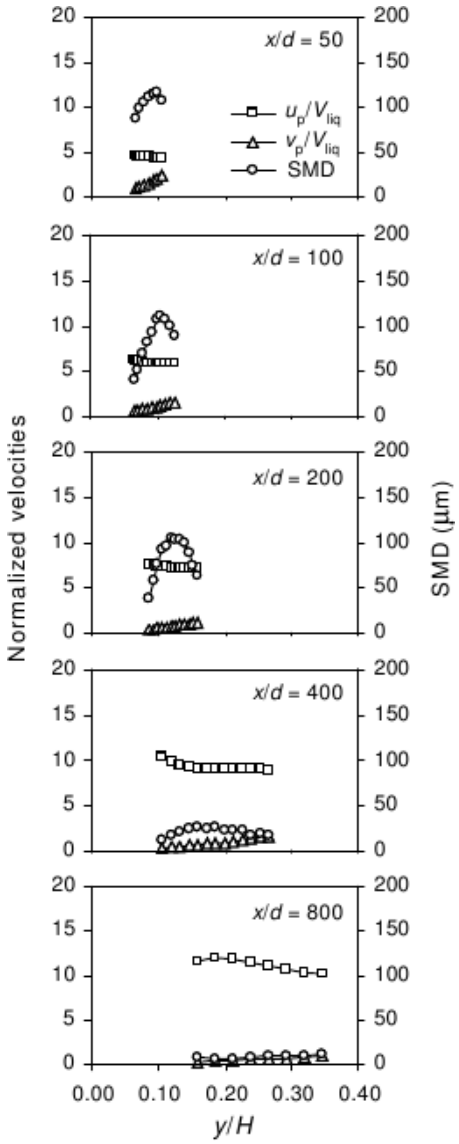


**Figure 8.** Normalized velocities and droplet size along the *y*-direction for test condition 4 ($\alpha$ = 90º) at $x/d$ = 50, 100, 200, 400 and 800.

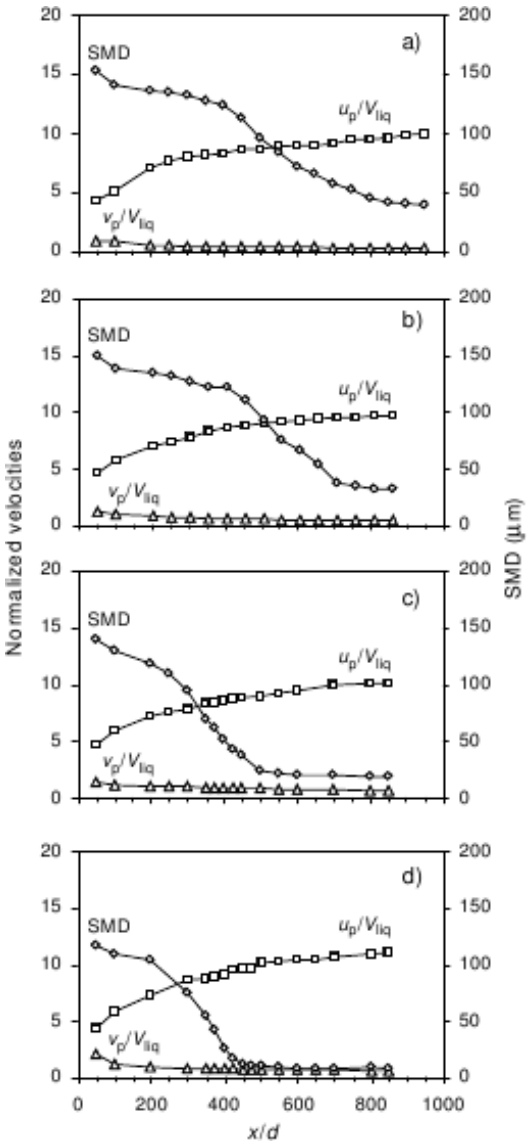


**Figure 9.** Normalized velocities and droplet size along the spray centerline: a) test condition 1; b) test condition 2; c) test condition 3; d) test condition 4.

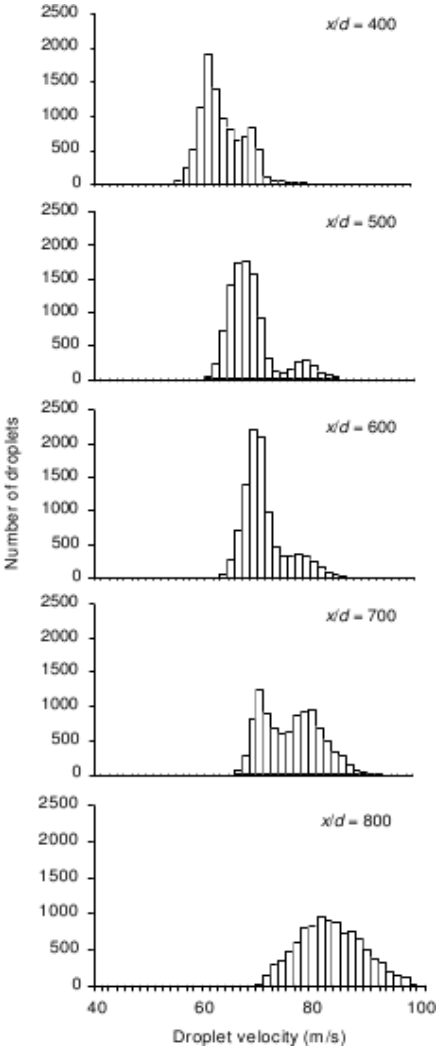


**Figure 20.** Droplet size distributions along the spray centerline for test condition 2 at $x/d$ = 400, 500, 600, 700 and 800.

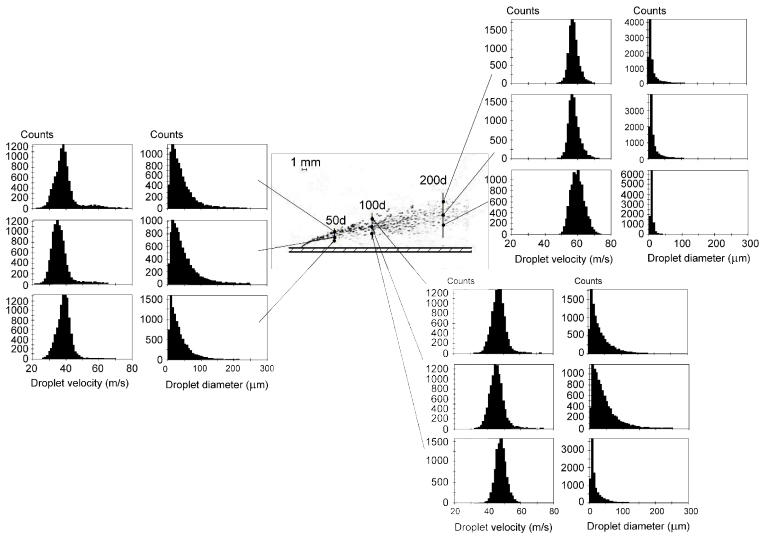


**Figure 31.** Droplet velocity and size distributions in various spray locations for test condition 2.